energies

*Article*

# Optical Properties of Coal after Ex-Situ Experimental Simulation of Underground Gasification at Pressures of 10 and 40 bar

**Jacek Nowak [1], Magdalena Kokowska-Pawłowska [1], Joanna Komorek [1], Marian Wiatowski [2,*], Krzysztof Kapusta [2] and Zdzisław Adamczyk [1]**

[1] Faculty of Mining, Safety Engineering and Industrial Automation, Silesian University of Technology, ul. Akademicka 2A, 44-100 Gliwice, Poland
[2] Główny Instytut Górnictwa (Central Mining Institute), Plac Gwarków 1, 40-166 Katowice, Poland
* Correspondence: mwiatowski@gig.eu; Tel.: +48-32-3246512; Fax: +48-32-2592267

**Abstract:** Coal gasification experiments were carried out in a reactor used to simulate underground coal gasification (UCG) processes under ex situ conditions at pressures of 10 and 40 bar. Changes in the optical properties of the organic matter were analyzed and the influence of temperature on coal during the UGC process was subsequently determined. The values of the true maximum reflectance determined for the gasification residue at pressures of 10 and 40 bar, and at distances of 0.75 and 1.75 m, reached a level corresponding to semi-graphite. Furthermore, it was found that the values of the true maximum reflectance and bireflectance decrease with increasing distance from the reactor chamber inlet. In addition, the results show that, regardless of the pressure used during the experiment, the temperature influence on the coal decreased with increasing distance from the reactor chamber inlet. The true temperatures operating during the experiment were higher than those recorded by the thermocouples, regardless of the pressure used. However, it was found that the distance at which the influence of temperature on the coal is still marked during the gasification process depends on the pressure used in the experiment. For example, in the case of the experiment at a pressure of 10 bar, the estimated distance is approximately 60 m, while for a pressure of 40 bar, it is approximately 35 m. These results can, and should, be taken into account for the planning of an UGC process.

**Keywords:** underground coal gasification (UCG); bituminous coal; oxygen gasification; reflectance; bireflectance



**Citation:** Nowak, J.; Kokowska-Pawłowska, M.; Komorek, J.; Wiatowski, M.; Kapusta, K.; Adamczyk, Z. Optical Properties of Coal after Ex-Situ Experimental Simulation of Underground Gasification at Pressures of 10 and 40 bar. *Energies* **2022**, *15*, 8824. https://doi.org/10.3390/en15238824

Academic Editor: Dameng Liu

Received: 2 November 2022
Accepted: 21 November 2022
Published: 23 November 2022



## 1. Introduction

The process of coal gasification has been around for over 200 years. It involves the conversion of coal into a process gas that can be used, for example, in the chemical industry as a synthesis gas or for obtaining hydrogen, which is considered to be the fuel of the future [1,2]. A number of chemical reactions take place in the coal gasification process, including oxidation, reduction, and distillation. As a result, heat is released, which causes the temperature to rise well above 1000 degrees Celsius.

Research has been carried out on underground coal gasification (UCG) for over a century [1,3–5]. Indeed, UCG is considered as an alternative to coal extraction, as well as a way to use deposit residues or thin coal seams that cannot be exploited with traditional mining methods for technical or economic reasons [6,7]. The use of UCG processes can also help minimize some of the environmental damage associated with traditional coal mining. These include no underground work, less impact on the surface (land subsidence and mining waste dumps), and increased efficiency in the use of coal, which improves the economic balance and simultaneously reduces overall emissions to the environment compared to conventional mining [6,7].

Regarding the industrial use of UCG, an important aspect is the type and range of impacts the process has on the rock mass surrounding the georeactor. These interactions cause changes in the coal and rocks surrounding the coal seam, which can lead to the formation of cracks and pores [8]. This creates the risk of uncontrolled gas migration and contamination of the surrounding groundwater [9–15]. Many experiments have been carried out (including gasification of hard coal and lignite, both in laboratory conditions simulating the coal seam, as well as in georeactors, that focused on the optimization of the process flow and the composition of the process gas obtained [4,16–23]. The gasification process also harnesses solid products, such as thermally transformed coal and mineral substances; however, these have garnered less research interest.

The organic matter (i.e., coal) is very sensitive to temperature. Under the influence of temperature, the petrographic composition of coal changes, as well as its properties, such as reflectance and chemical composition (i.e., the carbon content, C, hydrogen, H, and nitrogen, N).

The reflection of the temperature in the georeactor is the degree of organic matter carbonation, most often expressed by the reflectance value of vitrinite, which is one of the primary components of coal. A common result of coal thermal metamorphism is its transformation into anthracite or natural coke in the temperature-affected zone. Numerous studies have revealed changes in vitrinite reflectance related to the thermal metamorphism of coal caused by intrusions in the Upper Silesian Coal Basin, a region in southern Poland which also spans into Czechia [24–29]. Experimental studies were also carried out to determine the rate of change in the optical parameters of vitrinite with increasing temperature. They showed that, after short-term heating at 350–400 °C, the light reflectance and vitrinite birefringence changes begin [30–32]. Such changes in optical properties are related to thermal changes taking place in the internal structure of vitrinite and its transformation products (mesophases and matrix). The nature and intensity of these changes depend on the coal rank and coking susceptibility of the starting material [33–37].

Research conducted so far on the influence of temperature on the optical properties of vitrinite has revealed that the changes in the internal structure of vitrinite due to increasing temperature can be divided into two stages. In the first stage, which occurs between 400 and 600 °C, rapid changes in the parameters characterizing the internal structure of vitrinite annealing products were observed. In the vitrification derived from coking coal at temperatures of 500 °C or 600 °C, mesophase appears, which, at higher temperatures, transforms into the basic mass matrix. These changes are related to degassing and plasticizing processes. The second stage of changes was observed between 800 and 1200 °C. In this range, the mean reflectance $R_r$ and the bireflectance $R_{bi}$ of vitrinite further increase. This means that, with the increase in the annealing temperature, the order of the internal structure of vitrinite carbonization products increases [33,34,38,39].

Vitrinite reflectance is a very good indicator showing the intensity of changes taking place in the georeactor, as well as in its immediate surroundings. However, so far only a few publications have addressed the issues of changes in reflectance [40] or petrographic composition [41] in gasification residue (coal, carbonizate, rocks) created during UCG.

Previous work [8,42–44] on UCG concerned the analysis of the possibility of transforming the coal seam resources into gas that can be used as both fuel and for the production of electricity and chemicals. However, such experiments are costly compared to experiments performed in simulation reactors designed for these exact purposes. Gasification in a reactor simulating UCG does not require expensive mining work. The reactor can be used many times for experiments with different types of coal.

The coal rank, most often expressed by the vitrinite reflectance value, reflects the temperature acting on the organic substance. There are few known studies on the transformation of organic matter after UCG [40,41]; however, no such studies have been conducted after coal gasification in a simulation reactor. The aim of this study is to assess the impact and range of temperature influence on coal during the coal gasification process in a simulation reactor. The results of these studies may contribute to a deeper understanding of the

phenomena occurring during UCG processes in particular, to determine the range of the impact of UCG processes on the coal seam and surrounding rocks.

## 2. Experimental Methods

### *2.1. Reactor Construction and Sample Preparation*

Coal gasification was performed in a reactor used to simulate UCG processes ex situ. The scheme of the applied installation is presented in Figure 1. The reactor was constructed of a metal, heat-resistant pipe with an outer diameter of 0.9 m and a length of 3.5 m, insulated on both the inside and outside with heat-resistant material. The inside of the reaction chamber was constructed to create an artificial coal seam with a maximum length of approximately 3.5 m, with a cross-section of 0.42 m × 0.42 m. Depending on the type of coal, this corresponds to a charge to the reactor within the range of 500–800 kg.

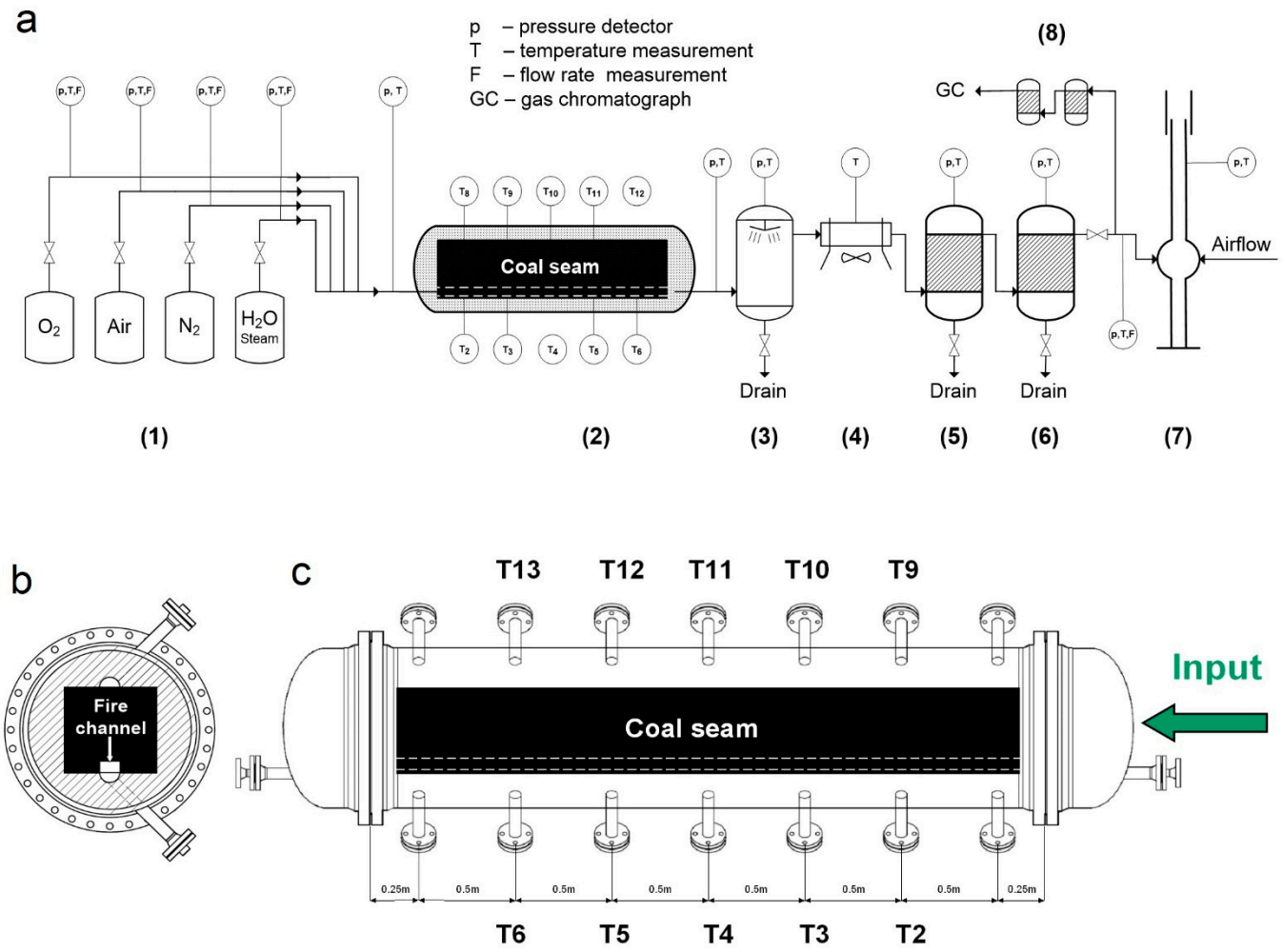


**Figure 1.** Reactor used in the experiment. (**a**) Scheme of the pressure unit for simulation of the underground coal gasification process, as follows: (1) compressed reagents, (2) pressure reactor, (3) wet scrubber, (4) air cooler, (5,6) gas cleaning system, (7) thermal combustor, (8) gas treatment module prior to GC analysis; (**b**) cross-section of the reactor, (**c**) longitudinal section of the reactor.

The reactor was closed on both sides with cylindrical ends. Pipes passed through both ends, which made it possible to supply the gasification agent to the interior of the reactor, as well as to discharge the gasification products. Gaseous media were supplied to the reactor by a system of metal pipes equipped with valves, sensors and flow regulators. Technical oxygen (99.5%) and nitrogen gas were taken from gas cylinders (Figure 1a), and a compressor supplied the compressed air.

Sensors were installed that measured the temperature and pressure of gases at the inlet and outlet of the reactor, the scrubber, and the purification module. The reactor was equipped with 14 spigots (7 at the bottom and 7 at the top) to measure the temperature in various places. For the purposes of these experiments, only 10 of them were used. Temperature measurements were carried out using a B-type thermocouple (PtRh30-PtRh6), and measurements were taken at the bottom of the reactor using thermocouples T2-T6, and at the top part of the reactor using thermocouples T8-T13. Reading the temperature inside the reactor allowed for continuous control of the gasification process during the experiment (Figure 1).

Before placing the block of coal in the reactor chamber, it was cut into blocks with transverse dimensions of 0.4 m × 0.4 m. The number of blocks was selected in such a way that their total length was 3.5 m. A hole with a square cross-section of 0.1 m × 0.1 m was cut in the lower part of the blocks which acted as a fire channel through which process gases could be transported to the reactor outlet (Figure 2).

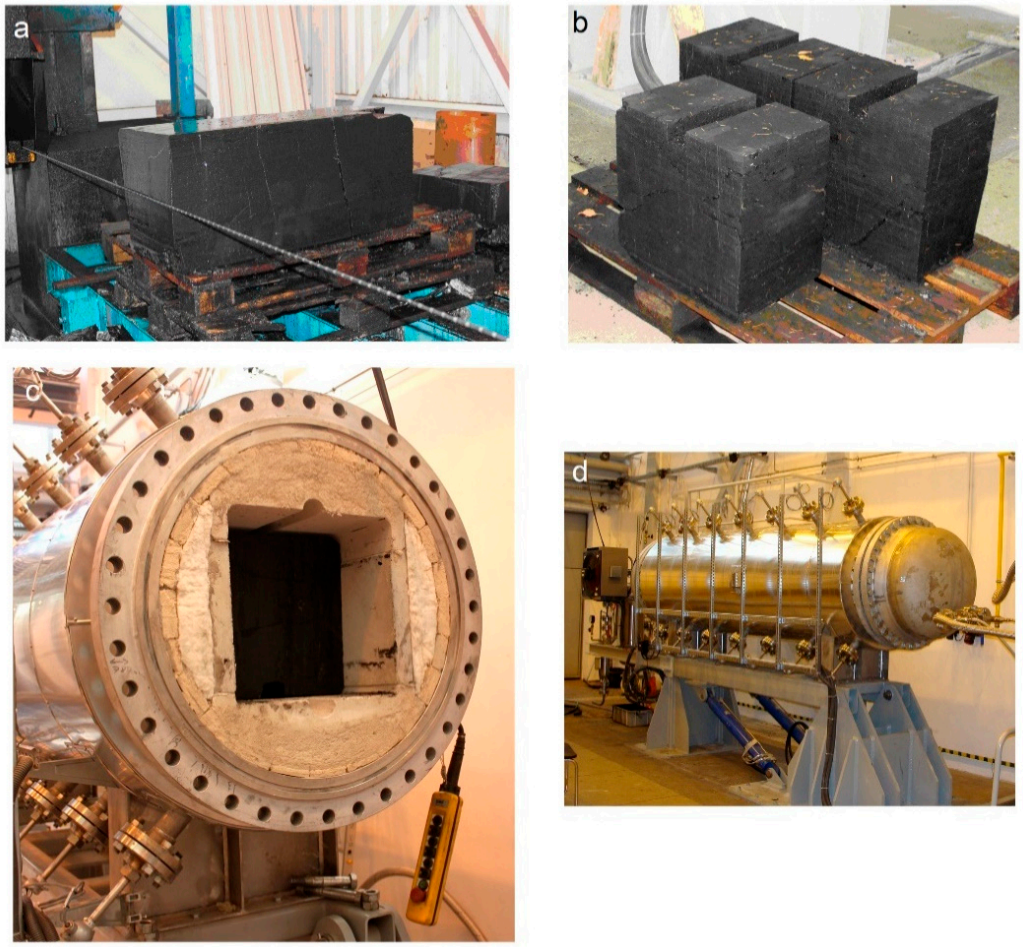


**Figure 2.** Preparation of coal for gasification. (**a**) Cutting block of coal, (**b**) coal blocks with a cut-out fire channel ready to be placed inside the reactor, (**c**) reaction chamber while loading with coal blocks, (**d**) reactor prepared for gasification.

### *2.2. Experiment Parameters and Sampling*

Two tests of hard coal gasification at pressures of 10 and 40 bar were carried out in this study. Coal samples were obtained from one of the mines located in the Upper Silesian Coal Basin (Poland). The gasifying agent was pure oxygen, and had a flow rate of 4 $Nm^3/h$. The duration of the experiments was 72 hours. An oxygen flow rate of 4 $Nm^3/h$ has been established experimentally based on earlier research and the chosen value depended mainly on the geometry of the reactor. At a higher oxygen flow rate, e.g., 6 $Nm^3/h$, oxygen

appeared in the process gases, and at a lower flow rate e.g., 2 $Nm^3/h$ the reactor heating time was very long. Therefore, the oxygen flow rate of 4 $Nm^3/h$ was determined as the optimal.

After loading the coal into the reactor, the whole installation was tested for any air leaks with compressed nitrogen. The coal was then ignited with a pyrotechnic charge at a distance of one meter from the beginning of the coal seam. The ignition of the coal was started in a stream of 2 $Nm^3/h$ of pure oxygen at atmospheric pressure, after which the oxygen pressure was slowly increased to 10 or 40 bar for the first and second experiments, respectively.

The beginning of the experiment was taken as the moment when the pressure inside the reactor reached the target value. Then, the oxygen flow was increased to 4 $Nm^3/h$, where it remained until the end of the experiment. At the end of the experiment, the oxygen flow was turned off and the pressure in the reactor was reduced to atmospheric value and cooled down using a nitrogen stream at a flow rate of 2 $Nm^3/h$. The cooling time was 4 days, after which samples were taken for analysis. Finally, after removing any gasification residue, the entire plant was prepared for the next experiment.

The research was based on a raw coal sample and six samples of gasification residues (three samples each for 10 bar and 40 bar pressure) taken at distances of 0.75, 1.75, and 2.75 m from the reaction chamber inlet, which correspond to thermocouple positions T9, T11, and T13.

The samples were reduced and ground to a fraction of $\varphi < 1$ mm, and briquettes of them were made for microscopic examination of the petrographic composition of the raw coal sample. In this way, the percentage content of macerals were determined. The analysis was performed in accordance with PN-ISO-7404-2:2005 [45].

### *2.3. Analyses Methods*

The optical properties of raw coal and gasification residues were analyzed, including the measurements of the average random vitrinite reflectance $R_r$ (according to PN-ISO 7404-5:2002 [46]) of raw coal, as well as its transformation products after the gasification process.

Random values of reflectance $R_{max}'$ and $R_{min}'$ were registered for each measurement point. Based on these results, using Kilby's method [47–49], a true maximum $R_{max}$ and minimum $R_{min}$ reflectance value was calculated. The value of optical anisotropy was expressed by means of bireflectance $R_{bi}$ given by the following:

$$R_{bi} = R_{max} - R_{min}$$

Microscopic examinations were carried out using a Zeiss optical light microscope equipped with a microphotometer. An immersion oil was used with a refractive index $n_o = 1.5176$ at 23 °C and light wavelength $\lambda = 546$ nm.

Chemical and technological analysis of the raw coal sample was performed, which included the following determinations: moisture content $W^a$ (PN-G-04560:1998 [50]), ash content $A^d$ (PN-G-04560:1998 [50]), volatile matter content $V^{daf}$ (PN-G-04516:1998 [51]), calorific value $Q_s{}^{daf}$ (PN-ISO 1928:2020-05 [52]) and total sulfur content (PN-G-04584:2001 [53]).

Elemental analysis ($C^{daf}$, $H^{daf}$, and $N^{daf}$) according to the PN-G-04571:1998 standard was performed for the raw sample as well as all samples of gasification residues. All analysis was carried out at the Silesian University of Technology, Gliwice, Poland.

## 3. Results

### *3.1. Properties of Raw Coal Sample before Gasification*

It was found that the raw coal sample had an ash content $A^d$ of 2.74%, moisture content $W^a$ of 2.36%, volatile matter content $V^{daf}$ of 32.61%, and a calorific value $Q_s{}^{daf}$ of 31.9 MJ/kg. The sulfur content $S_t{}^d$ in the tested sample was small and amounted to only 0.31%.

The results of the elemental analysis indicate that the content of $C^{daf}$ in the tested coal sample was 81.74%, while the shares of hydrogen $H^{daf}$ and nitrogen $N^{daf}$ were 4.39% and 1.3%, respectively (Table 1).

**Table 1.** Chemical–technological properties and vitrinite reflectance of a raw coal sample.

| **Chemical–Technological Properties** | | | | | | | | |
|---|---|---|---|---|---|---|---|---|
| $W^a$ | $A^d$ | $V^{daf}$ | $Q^{daf}$ | $S_t^d$ | $C^{daf}$ | $H^{daf}$ | $N^{daf}$ | |
| % | % | % | MJ/kg | % | % | % | % | |
| 2.36 | 2.74 | 32.61 | 31.9 | 0.31 | 81.74 | 4.39 | 1.3 | |
| **Optical Properties** | | | | | | | | |
| $R_r$ | S | $R_{max}$ | $s_{max}$ | $R_{min}$ | $s_{min}$ | $R_{rmax}$ | $R_{rmin}$ | $R_{bi}$ |
| % | % | % | % | % | % | % | % | % |
| 0.79 | 0.05 | 0.82 | 0.03 | 0.76 | 0.05 | 0.88 | 0.66 | 0.22 |

Abbreviations are as follows: $R_r$, mean random reflectance; s, standard deviation of $R_r$ value; $R_{max}$, mean maximum reflectance; $R_{min}$, mean minimum reflectance; $s_{max}$, standard deviation of $R_{max}$ value; $s_{min}$, standard deviation of $R_{min}$ value; $R_{rmax}$, true maximum reflectance value; $R_{rmin}$, true minimum reflectance value; $R_{bi}$, bireflectance.

The tested coal was characterized by an average vitrinite reflectance $R_r$ = 0.79%, with the standard deviation s = 0.05%.

The analysis of the optical properties of the raw coal sample showed that the maximum mean $R_{max}$ and minimum $R_{min}$ reflectance values of vitrinite were 0.82% and 0.76%, respectively, with standard deviations of 0.03% and 0.05%, respectively. The value of the true maximum reflectance, $R_{rmax}$, determined on the basis of Kilby diagrams, was 0.88%, while the true minimum reflectance, $R_{rmin}$, was 0.66%. The bireflectance $R_{bi}$ was found to be 0.22% (Table 1).

The analysis of macerals groups showed that the vitrinite content in the analyzed raw coal sample was 47% (Figure 3). Among the vitrinite group, colodetrinite and colotelinite the most commonly were observed. Corpogelinite was only occasionally observed (as shown in Figure 4a,b,d).

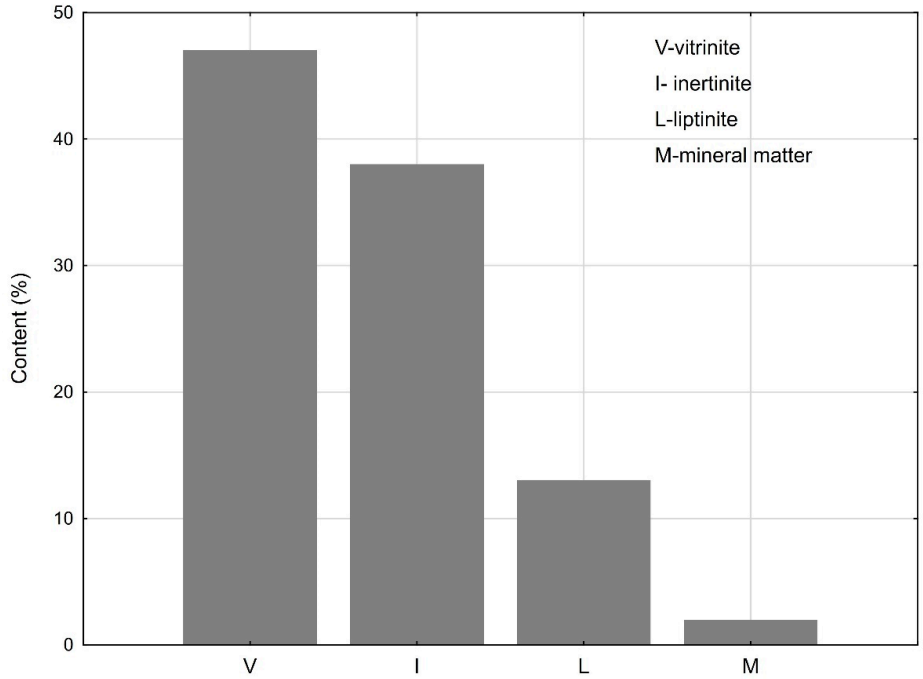


**Figure 3.** Petrographic composition of the raw sample.

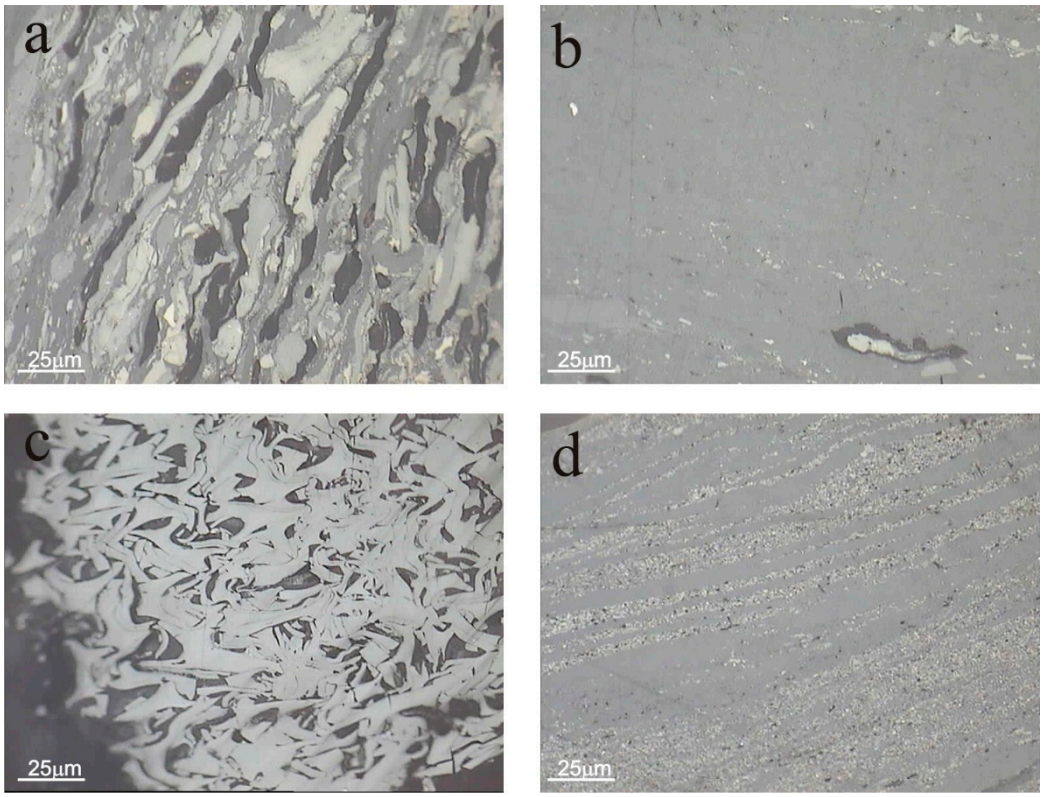


**Figure 4.** Raw sample of coal showing (**a**) trimacerite, (**b**) vitrinite–collotelinite, (**c**) inertinite–semifusinite, and (**d**) vitrinertite–collodetrinite and micrinite.

The content of macerals in the liptinite group was found to be 13% (Figure 3), with the most frequently observed maceral in the liptinite group being sporinite in the form of macro- and microspores. Cutinite, resinite, and liptodetrinite were found in much smaller amounts (Figure 4a).

The share of macerals from the inertinite group was 38% (Figure 3). This group was represented by inertodethrinite semifusinite and micrinite, where micrinite and fusinite were found to be less common (Figure 4a–d).

The content of the mineral substance in the tested coal sample was low and amounted to only 2%. The mineral matter was mainly represented by carbonates, iron sulfides, and the polymineral substance.

Based on the results obtained, the raw coal sample was classified as low ash ($A^d < 10\%$), medium vitrinite (vitrinite content in mineral matter free state $40\% < V^{mmf} < 60\%$), and medium rank bituminous C coal (PN-ISO 11760:2007 [54]).

### *3.2. Temperature Distribution in the Reactor during Gasification*

The temperature distribution in the reactor chamber during the coal gasification experiments at 10 and 40 bar pressures was analyzed. It was found that in both experiments the recorded temperature at the distances of 0.75 m (T9 and T2 thermocouples), 1.75 m (T11 and T4 thermocouples), and 2.75 m (T13 and T6 thermocouples) in the top and bottom parts, respectively, was different during the entire gasification process (Figures 5 and 6).

The highest recorded temperature at a distance of 0.75 m at a pressure of 10 bar was about 1000 °C in the top part and 580 °C in the bottom part (thermocouples T9 and T2, respectively). As the distance from the reactor chamber inlet increased, the values of the recorded temperatures decreased. At a distance of 1.75 m from the reactor chamber inlet, the highest recorded temperatures are 880 °C and 300 °C in the top and bottom parts, respectively (thermocouples T11 and T4, respectively). The highest temperature recorded by thermocouples T13 and T6, located 2.75 m from the reactor chamber inlet, was

approximately 580 °C in the top part and 280 °C in the bottom part, respectively (Figure 5a and Figure 5b, respectively).

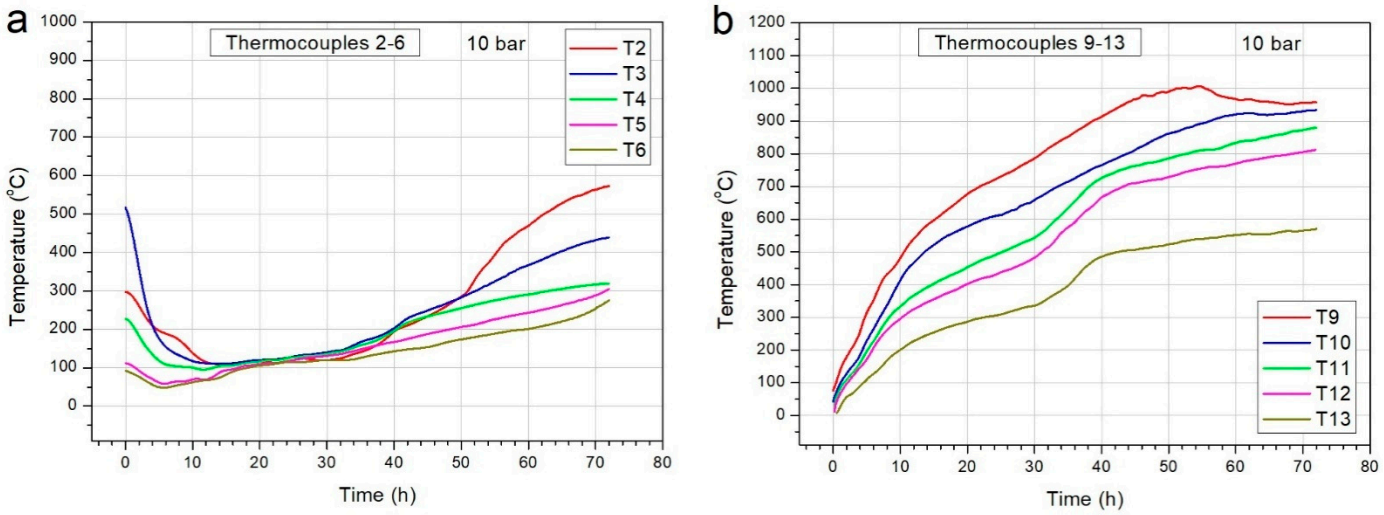


**Figure 5.** Temperature distribution during gasification of coal under 10 bar pressure. (**a**) Bottom part of the reactor and (**b**) the top part of the reactor.

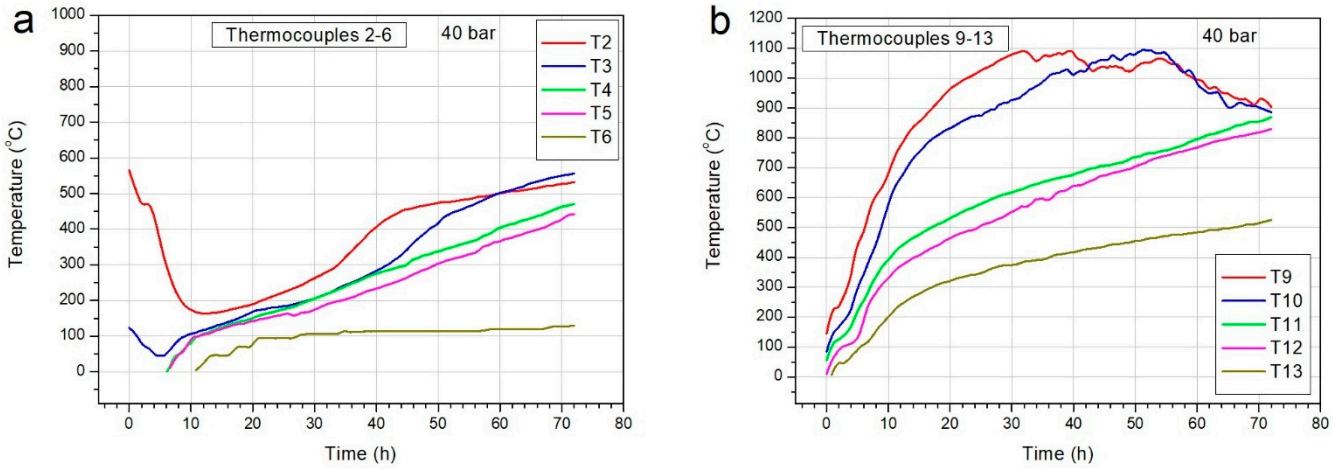


**Figure 6.** Temperature distribution during gasification of coal under 40 bar pressure. (**a**) Bottom part of the reactor and (**b**) the top part of the reactor.

During the experiment carried out at a pressure of 40 bar, the highest temperature in the top part was approximately 1100 °C and 550 °C in the bottom part, respectively (thermocouples T9 and T2, respectively, at distance d = 0.75 m).

As the distance from the reactor chamber inlet increased, the recorded temperature values decreased. At a distance of 1.75 m, the highest recorded temperature is 875 °C and 450 °C in the top and bottom part, respectively (thermocouples T11 and T4, respectively). The highest temperature recorded by thermocouples T13 and T6, located 2.75 m from the reactor chamber inlet, was approximately 520 °C in the top part and 120 °C in the bottom part, respectively (Figure 6a and Figure 6b, respectively).

Based on the results obtained, it can be concluded that the temperature in the bottom part of the reactor was much lower compared to the temperature in the top part, regardless of the pressure used during gasification. This is a result of the lower thermocouples being insulated by the ash and slag formed during gasification. Therefore, during the analysis of the residues after coal gasification, the maximum temperatures recorded by thermocouples from the roof layer were taken into account.

The distance of the thermocouples from the top and bottom part of the reactor chamber was about 2 cm. This positioning of the thermocouples was necessary to protect them from direct contact with the oxidants used during coal gasification. Therefore, the true temperature of the gasification process was probably about 100–200 °C higher. However, due to insulating phenomena (used refractory materials and ceramic thermocouple sheaths), the recorded temperature was lower (Figures 1, 2, 5 and 6).

As can be seen in the diagrams (Figures 5 and 6), the temperature increases the fastest in the initial section of the reactor (near the oxygen input). This is due to the fact that the gasification process was initiated at this point (ignition site). With time, the intensity of the gasification process also increases in the further part of the reactor, which is illustrated by the increase in temperature recorded by successive thermocouples.

Higher pressure (40 bar) resulted in a faster temperature increase in the reactor during the experiment. Higher maximum temperatures were also obtained. After the 55th hour of the experiment, a clear decrease in the temperature measured by thermocouples T9 and T10 is observed. This means that the coal in this part of the reactor has already been gasified and the intensity of the reaction has begun to decrease.

### *3.3. Properties of Residues after Coal Gasification*

#### 3.3.1. Elemental Analysis

The results of the elemental analysis of the coal gasification residue indicate that the coal gasification products at a pressure of 10 bar show a similar $C^{daf}$ content in the range of 90.93% to 92.19%. However, coal gasification at a pressure of 40 bar caused the content of $C^{daf}$ in the tested samples to reach values in a range from 88.98 to 93.90%.

The share of $C^{daf}$ in all analyzed gasification residue samples is higher than in the raw sample, where the highest $C^{daf}$ content was found in the sample taken at a distance of 0.75 m from the inlet of the reaction chamber. On the other hand, the lowest $C^{daf}$ content was found in the sample taken at a distance of 2.75 m from the inlet of the reaction chamber (Tables 1 and 2, and Figure 7).

**Table 2.** The results of elemental analysis of residues after coal gasification.

| Pressure | Sample | d | $C^{daf}$ | $H^{daf}$ | $N^{daf}$ |
|---|---|---|---|---|---|
| Bar | | m | | % | |
| 10 | 10-1 | 0.75 | 90.93 | 0.83 | 1.08 |
| | 10-2 | 1.75 | 92.19 | 0.68 | 1.40 |
| | 10-3 | 2.75 | 91.09 | 0.98 | 1.43 |
| 40 | 40-1 | 0.75 | 93.90 | 0.58 | 1.09 |
| | 40-2 | 1.75 | 92.56 | 1.15 | 1.54 |
| | 40-3 | 2.75 | 88.98 | 2.38 | 1.39 |

Abbreviations are as follows: d, distance from reactor chamber inlet.

On the basis of the presented results, it can be concluded that the $C^{daf}$ content in the gasification residue was about 10% higher than in the raw coal sample.

#### 3.3.2. Optical Properties of the Residue after Gasification at a Pressure of 10 Bar

Microscopic observations of coal samples subjected to gasification at 10 bar pressure showed that they contain coal components that have been transformed under the influence of temperature. Vitrinite grains were found with visible pores after degassing (Figure 8a), and coke grains were also observed in these sample, which are characterized by the presence of various pore sizes with a high relief (Figure 8b). There was also a mesophase, where, in some places, it formed regions of the same optical orientation anisotropic domains (Figure 8c–f). The morphology of the macerals of the liptinite group changed significantly compared to the raw sample; the edges of some grains were rounded, and the color became lighter than in the raw sample (Figure 8e). Despite these changes, it was found that the

degree of change in the morphology of the coal components caused by the influence of temperature decreased as the distance from the reactor chamber inlet increased.

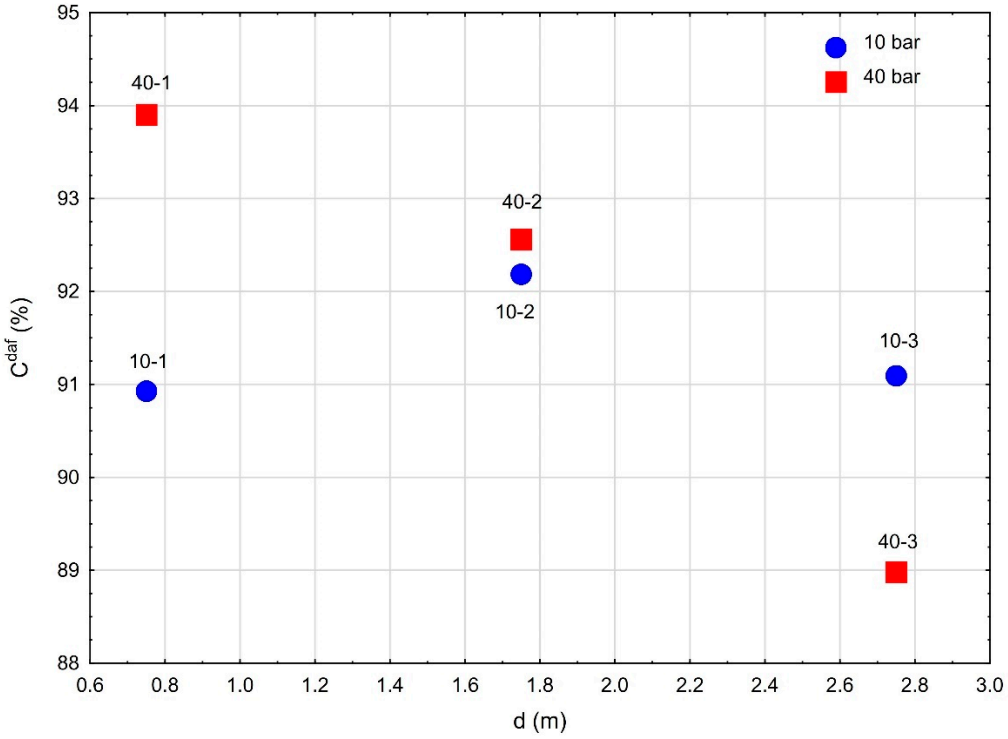


**Figure 7.** Relationship between $C^{daf}$ content and distance from the reactor chamber inlet.

Microscopic observations of the samples subjected to coal gasification at a pressure of 10 bar revealed that the optical properties of coal petrographic components changed during this process. This means a change in the coal rank of the gasification residue compared to the raw coal sample.

In order to determine the rank of coal, the reflectance of vitrinite and products of its thermal transformations was measured.

Gasification products at a pressure of 10 bar were characterized by a different coal rank. The mean maximum $R_{max}$ reflectance value determined for them ranged from 5.29% to 6.28%, with the standard deviation $s_{max}$ between 0.55% and 1.07% (Figure 9a).

The mean minimum $R_{min}$ reflectance value varied from 4.66% to 5.40%, with the standard deviation of $s_{min}$ ranging from 0.59% to 1.07%.

Such a high value of this parameter could have been influenced by the changing temperature in the reactor chamber during the experiment. For this reason, for the gasification products at a pressure of 10 bar, the true values of maximum $R_{rmax}$ and minimum $R_{rmin}$ reflectance were determined using Kilby's method.

Kilby diagrams for samples taken from 0.75m and 1.75m were very clear. However, in the case of the sample taken from a distance of 2.75 m, two populations of reflectance values were distinguished. The first one included $R_{max}$ values < 3.5%. In this interval of reflectance, the Kilby diagrams were disordered and impossible to interpret. The second population had $R_{max}$ values > 3.5%, where, in this case, the Kilby diagram was clear.

The true maximum reflectance values $R_{rmax}$, calculated from the Kilby diagram, varied from 6.46% to 8.30%, whereas that true minimum reflectance $R_{rmin}$ ranged from 2.84% to 3.73%.

The bireflectance $R_{bi}$ varied from 3.36% to 4.57%, where the values of the true maximum reflectance $R_{rmax}$ determined for samples 10-1 and 10-2 reached the value corresponding to semi-graphite (6.5–9.0%) (Table 3, Figure 9b,d). Such a degree of transformation of the organic substance is confirmed by the value of the quotient H/C < 0.15 determined for these samples.

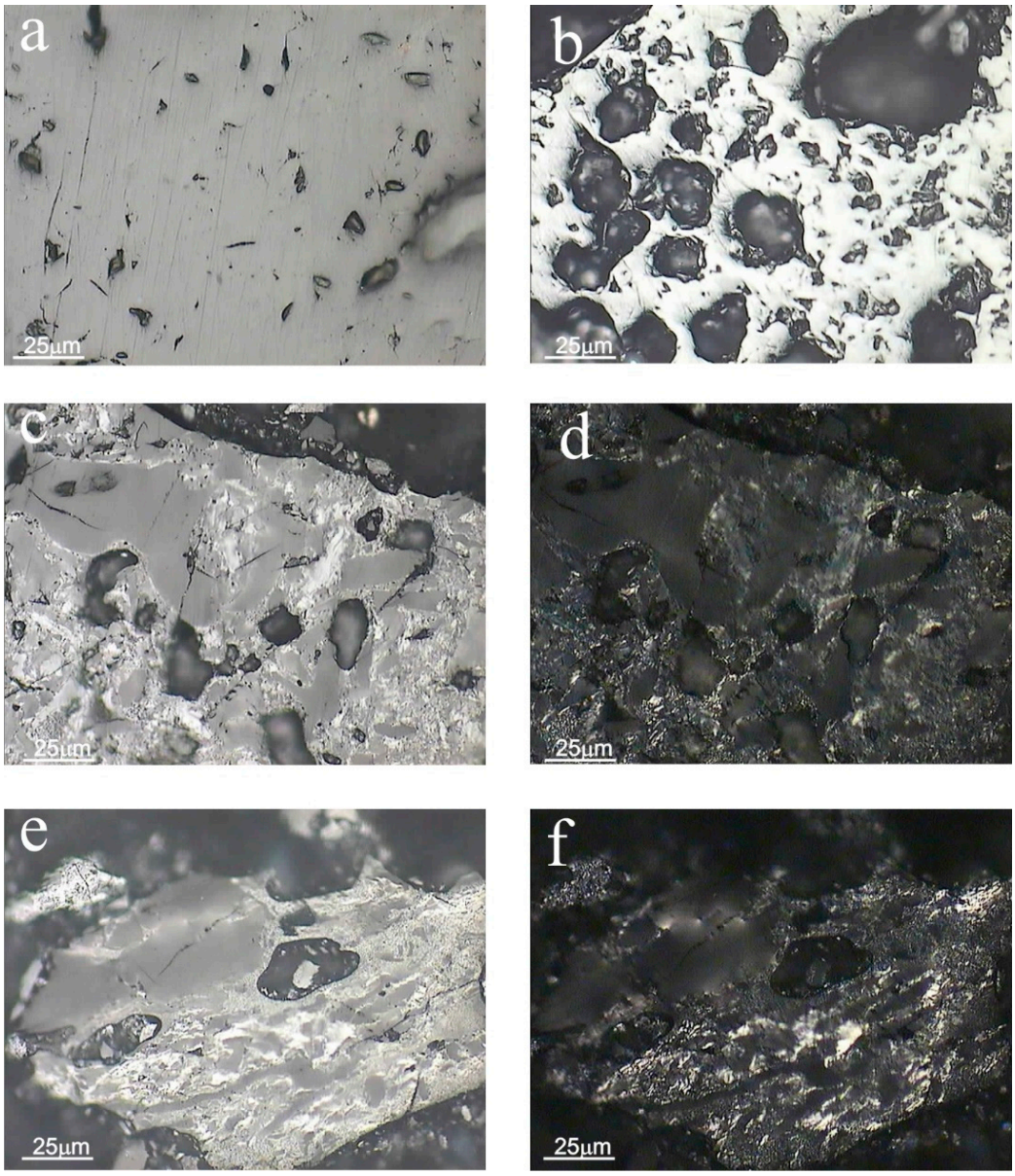


**Figure 8.** The residue after gasification of coal at a pressure of 10 bar. (**a**) Vitrinite with pores after degassing is visible; (**b**) heat-altered coal–coke structure is visible; (**c**) heat-altered coal–mesophase is visible (parallel nicols); (**d**) the same field as photo c (crossed nicols); (**e**) heat-altered coal–mesophase and thermally-altered liptinite is visible (parallel nicols); (**f**) the same field as photo e–(crossed nicols).

The results of this experiment show that with the increase in the distance from the reactor chamber inlet, the values of the true maximum reflectance and bireflectance decrease. These changes are related to the changing temperature in the reactor chamber during the experiment (Figure 9b,d).

3.3.3. Optical Properties of the Residue after Gasification at a Pressure of 40 Bar

Microscopic observations of coal samples subjected to gasification at 40 bar pressure showed that they contain coal components transformed under the influence of temperature.

Vitrinite grains were found with visible pores after degassing (Figure 10a), while coke grains were also observed in these samples and were characterized by the presence of various pore sizes and a high relief (Figure 10b). There was also a mesophase, where, in some places, it formed regions of the same optical orientation anisotropic domains (Figure 10c,d).

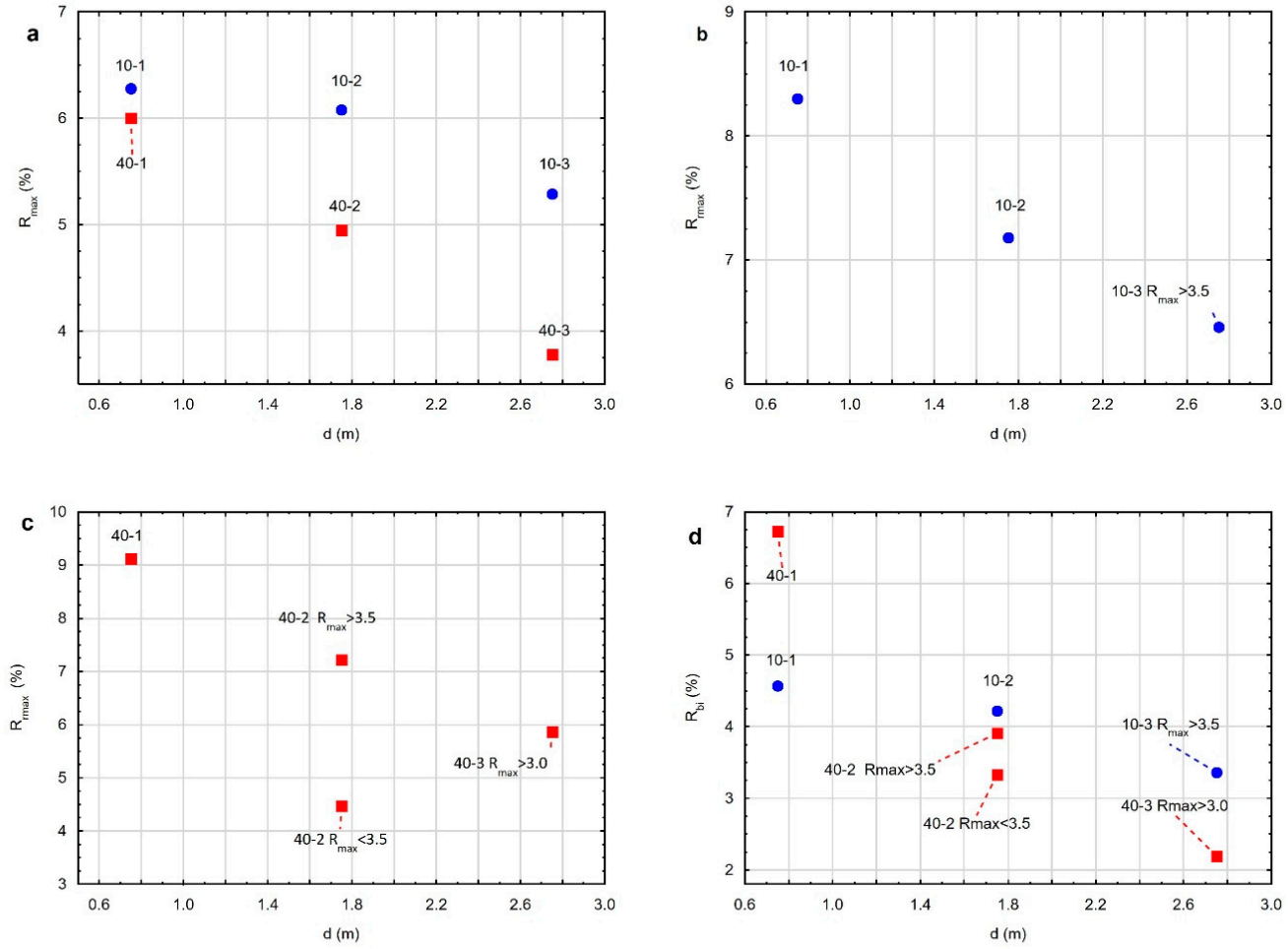


**Figure 9.** Relationship between (**a**) $R_{max}$; (**b**) $R_{rmax}$ (pressure of 10 bar); (**c**) $R_{rmax}$ (pressure of 40 bar); (**d**) $R_{bi}$ and distance d from the reactor chamber inlet.

**Table 3.** Characteristics of the optical properties of the raw sample and the residues after coal gasification.

| Pressure | Sample | | $R_{max}$ | $s_{max}$ | $R_{min}$ | $s_{min}$ | $R_{rmax}$ | $R_{rmin}$ | $R_{bi}$ |
|---|---|---|---|---|---|---|---|---|---|
| bar | | | | | | % | | | |
| 10 | 10-1 | AM | 6.28 | 1.01 | 4.87 | 1.07 | 8.30 | 3.73 | 4.57 |
| | 10-2 | AM | 6.08 | 0.55 | 5.40 | 0.59 | 7.18 | 2.84 | 4.22 |
| | 10-3 | AM | 5.29 | 1.07 | 4.66 | 1.07 | NM | NM | NM |
| | | $R_{max}$ < 3.5 | 2.76 | 0.60 | 2.29 | 0.55 | NM | NM | NM |
| | | $R_{max}$ > 3.5 | 5.32 | 0.57 | 4.72 | 0.81 | 6.46 | 3.10 | 3.36 |
| 40 | 40-1 | AM | 6.00 | 1.56 | 4.95 | 1.28 | 9.12 | 2.39 | 6.73 |
| | 40-2 | AM | 4.95 | 1.51 | 4.31 | 1.57 | NM | NM | NM |
| | | $R_{max}$ < 3.5 | 2.93 | 0.77 | 2.24 | 0.55 | 4.47 | 1.14 | 3.33 |
| | | $R_{max}$ > 3.5 | 5.82 | 0.70 | 5.21 | 0.85 | 7.22 | 3.31 | 3.91 |
| | 40-3 | AM | 3.78 | 1.84 | 3.45 | 1.7 | NM | NM | NM |
| | | $R_{max}$ < 3.0 | 1.34 | 0.38 | 1.19 | 0.37 | NM | NM | NM |
| | | $R_{max}$ > 3.0 | 5.09 | 0.39 | 4.60 | 0.46 | 5.87 | 3.68 | 2.19 |

Abbreviations are as follows: RS, raw sample; NM, not marked; AM, all measurements; $R_{max}$, mean maximum reflectance; $R_{min}$, mean minimum reflectance; $s_{max}$, standard deviation of $R_{max}$ value; $s_{min}$, standard deviation of $R_{min}$ value; $R_{rmax}$, true maximum reflectance value; $R_{rmin}$, true minimum reflectance value; $R_{bi}$, bireflectance.

The macerals of the liptinite group were characterized by a different degree of transformation. In the samples from a distance of 0.75 m and 1.75 m from the reactor chamber inlet, the color of liptinite was brighter than in the raw sample. In the sample coming from a distance of 2.75 m, grains were found, in which the color and morphology of liptinite showed almost no change compared to the raw sample (Figure 10e,f). The changes in the morphology of the coal components caused by the influence of temperature decreased as the distance from the reactor chamber inlet increased.

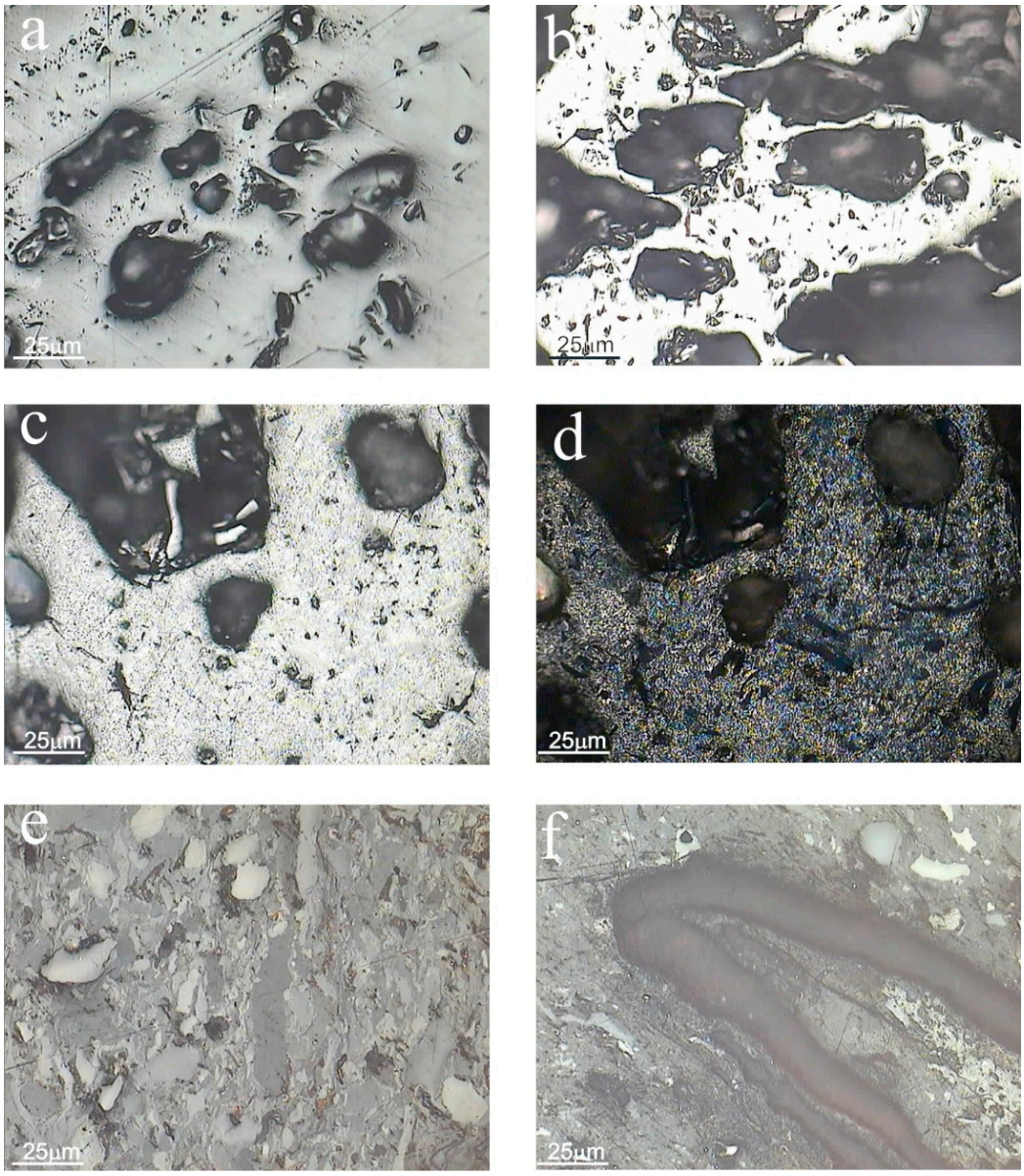


**Figure 10.** The residue after gasification of coal at a pressure of 40 bar. (**a**) Vitrinite with pores after degassing is visible; (**b**) heat-altered coal–coke structure is visible; (**c**) heat-altered coal–mesophase (matrix) is visible (parallel nicols); (**d**) the same field as photo c(crossed nicols); (**e**) trimacerite with the color and morphology of liptinite unchanged compared to the raw sample; (**f**) macrosporinite with the color and morphology of liptinite unchanged compared to the raw sample.

The mean maximum $R_{max}$ value of reflectance determined for the gasification residue under 40 bar pressure ranged from 3.78% to 6.00%, with a standard deviation ranging from 1.51% to 1.84%. The mean minimum $R_{min}$ reflectance value varied from 3.45% to 4.95%, with the standard deviation of $s_{min}$ ranging from 1.28% to 1.70% (Table 3, Figure 9a).

The Kilby diagram for the sample taken from 0.75 m was clear. The values of the true maximum, minimum reflectancs, and bireflectance for this sample were 9.12%, 2.39%, and 6.73%, respectively.

In the case of the remaining samples, two populations of reflectance values were distinguished; the first one included values in the range of $R_{max}$ < 3.5% (sample 40-2) and $R_{max}$ < 3.0% (sample 40-3). The second population included values $R_{max}$ > 3.5% and $R_{max}$ > 3.0% for samples 40-2 and 40-3, respectively. Kilby diagrams for both populations from sample 40-2 taken from a distance of 1.75 m from the reactor chamber inlet were very clear.

The true values of maximum and minimum reflectance and bireflectance were 4.47%, 1.14%, and 3.33%, respectively, for the $R_{max}$ < 3.5% population. The second population had the true values of maximum and minimum reflectance and bireflectance of 7.22%, 3.31%, and 3.91%, respectively.

The Kilby diagram for the sample taken at a distance of 2.75 m, in the reflectance range $R_{max}$ < 3.0%, was disordered and impossible to interpret. In contrast, the Kilby diagram for the second population of data, including reflectance values $R_{max}$ > 3.0%, was very clear.

The true values of maximum and minimum reflectance were 5.87% and 3.68%, respectively, and the bireflectance was 2.19%. The values of the true maximum reflectance $R_{rmax}$ determined for samples 40-1 and 40-2 ($R_{max}$ > 3.5% population) reached the level corresponding to semi-graphite (6.5–9.0%) (Table 3, Figure 9c,d). Such a degree of transformation of the organic substance is confirmed by the value of the quotient $H/C \leq 0.15$ determined for these samples.

The results of this experiment show that with the increase in the distance from the reactor chamber inlet, the values of the true maximum reflectance and bireflectance decrease. These changes are related to the changing temperature in the reactor chamber during the experiment (Figure 9c,d).

### *3.4. Maximum Temperature and Range of the Coal Gasification Process*

The calculated values of true maximum reflectance of the thermally transformed residue after coal gasification were used to estimate the maximum temperature that acted on the organic matter during the gasification experiments.

The values of true maximum reflectance gasification residue/vitrinite were compared with the data obtained for vitrinite subjected to thermal treatment in the laboratory experiments within the range of 400 °C to 1200 °C [37,39]. The arithmetic mean and standard deviation of the true maximum reflectance of vitrinite were calculated for each heat treatment temperature (i.e., 400, 500, 600, 800, 1000, and 1200 °C). The relationship between temperature and the mean value of the true maximum vitrinite reflectance $R_{max}$ = f(T) was then determined. This relationship was found to be linear and is given by $R_{rmax}$ = 0.00982T-2.6698 (r = 0.99, $p < 0.05$; see Figure 11). This function was then used to obtain the temperature that acted on the coal during the experiment.

It was calculated that, at a distance of 0.75 m from the reactor chamber inlet during the experiment at 10 bar pressure (sample 10-1), the temperature reached a value of at least 1119 °C (Figure 11). Temperatures of about 1005 °C (sample 10-2, d = 1.75 m) and 932 °C (sample 10-3, d = 2.75 m) influenced the samples located further from the reactor chamber inlet. During the experiment at a pressure of 40 bar, the maximum temperature was 1203 °C (sample 40-1, d = 0.75 m). The samples located at a greater distance were influenced by temperatures of about 1009 °C (sample 40-2, d = 1.75 m) and 871 °C (sample 40-3, d = 2.75 m) (Figure 11). The results of this experiment show that with the increase in the distance from the reactor chamber inlet, the values of the temperature decrease, regardless of the pressure applied during the experiment (Figure 12a,b).

The results obtained indicate that the maximum temperature influencing the coal during gasification was higher than the temperature recorded by the thermocouples. In the case of an experiment at a pressure of 10 bar, the difference between the temperature

recorded by the thermocouples and the temperature estimated on the basis of the reflectance measurements ranges from 120 to 350 °C.

The greatest temperature difference was found at a distance of 2.75 m from the reactor inlet (Figure 12a). Similar differences between the temperature recorded by thermocouples and the temperature estimated on the basis of the reflectance measurements were found for the experiment carried out at a pressure of 40 bar. These differences also range from about 100 to 350 °C at a distance of 2.75 m from the reactor inlet (Figure 12b).

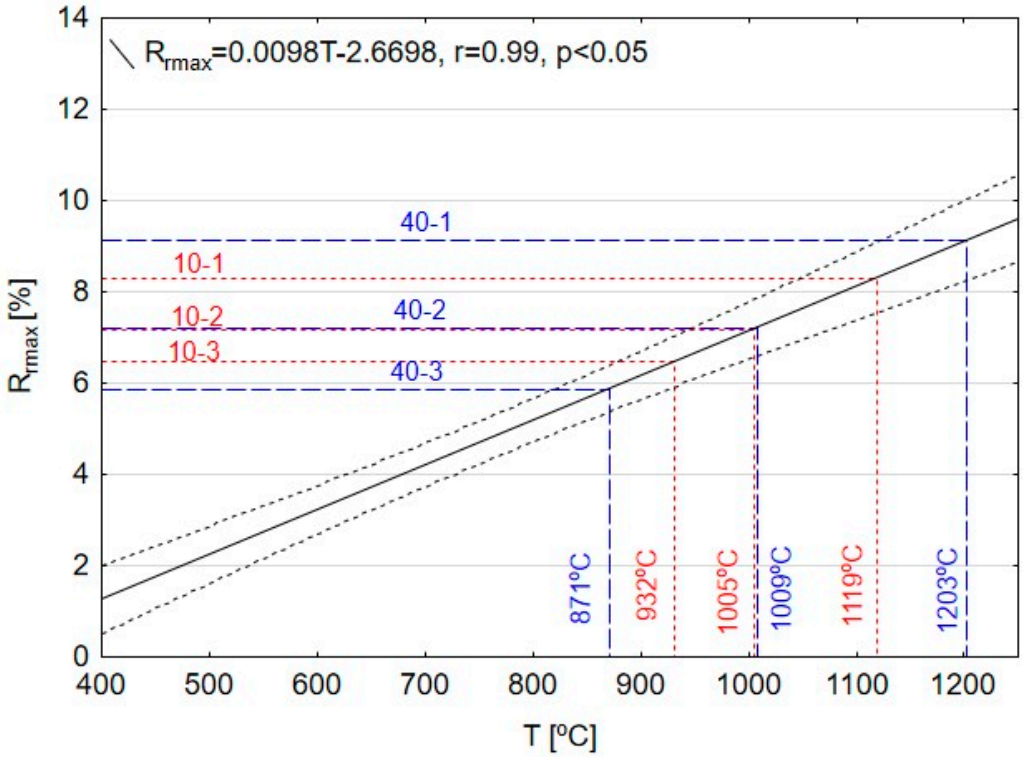


**Figure 11.** Comparison of maximum vitrinite reflectance with the data obtained for cokes produced in laboratory conditions [37,39].

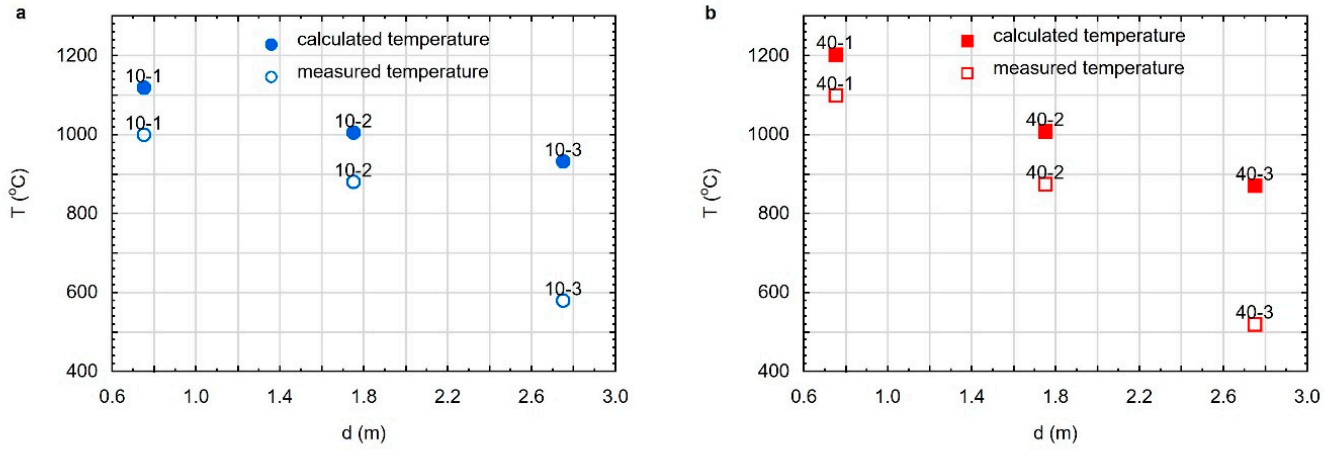


**Figure 12.** Relationship between measured and calculated temperature and distance from reactor chamber inlet at (**a**) pressure of 10 bar, and (**b**) pressure of 40 bar.

It was found that as the distance from the reactor chamber inlet increased, the values of the maximum temperature acting on the coal during gasification decreased.

This is confirmed by the observed values of the real maximum reflectance and bireflectance, which decreased with distance. This is because the degree of organic matter coalification (rank), expressed by the vitrinite reflectance value reflects the temperature

acting on the organic substance [55]. Similar changes in optical properties and the structure of residues after coal gasification were also observed in previous studies [40,41,56,57].

The obtained test results indicate that with the increase in the distance from the inlet of the reactor chamber, the value of the true maximum reflectance decreases.

There was an attempt made to estimate the distance from the reactor chamber inlet at which no increase in reflectance value was observed in relation to the raw sample.

For this purpose, the value of the reflectance ratio IR was calculated. The IR is the ratio of the true values of the maximum reflectance of the raw sample to the gasification residue.

It was found that with increasing distance from the reactor chamber inlet, both at 10 and 40 bar pressure, the value of the IR quotient increased systematically (Figure 13a,b). This is probably due to the differences in the maximum temperature reached in different parts of the reactor.

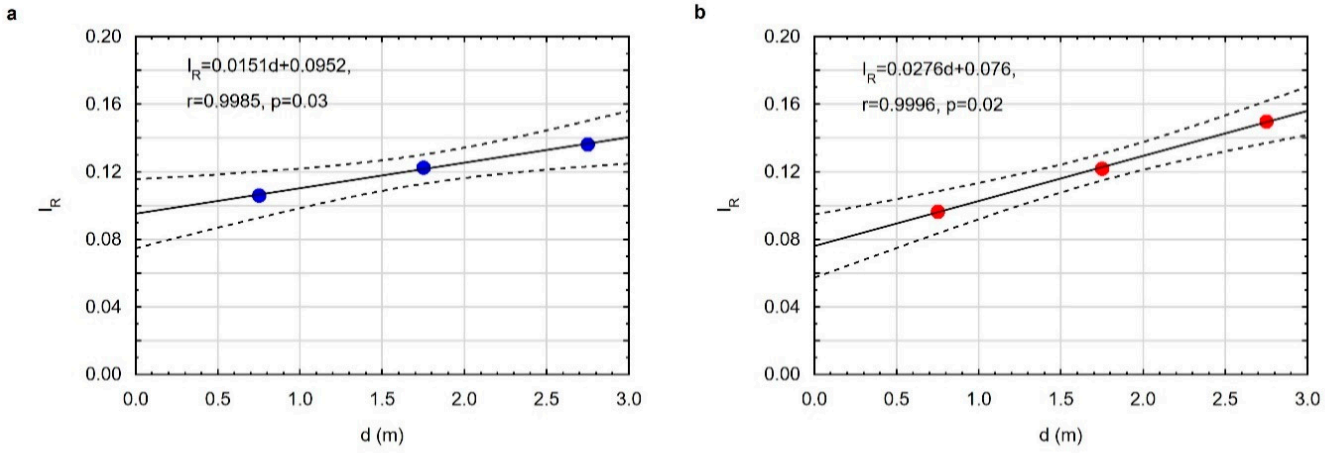


**Figure 13.** Relationship between $I_R$ ratio and distance from reactor chamber inlet at (**a**) pressure of 10 bar, and (**b**) pressure of 40 bar.

The distance for which the value of IR = 1 means that the reflectance value of the gasification residue is equal to that of the raw sample. In the case of an experiment at a pressure of 10 bar, the estimated distance for which IR = 1 is approximately 60 m, while for a pressure of 40 bar it is approximately 35 m, assuming that the relationship IR = f (d) is linear.

The obtained results show that the distance at which the temperature effect on the coal is marked during the gasification process depends on the pressure used in the experiment.

It should be noted that this distance was estimated only on the basis of the reflectance data from the ex situ gasification experiment. That distance in the mine conditions corresponds to the region of the UCG cavity and the boundary of the UCG cavity.

The exact distance depends on specific site geology, project scale, gasifier design, and operational parameters, and the calculated distance may correspond to the near field zone described by Perkins. This near field is a zone around the immediate cavity which is impacted by the presence of the UCG process, which undergoes chemical, thermal, geomechanical, and hydrogeological impacts. The region of the near field zone is expected to extend from tens to hundreds of meters from the center of the UCG cavity.

## 4. Conclusions

The gasification residues of medium rank bituminous C coal with low ash content and medium vitrinite content in a reactor at pressures of 10 bar and 40 bar showed about 10% higher $C^{daf}$ content than raw coal, with the lowest values occurring at the greatest distance from the reaction chamber inlet.

Regardless of the pressure in the gasification residues, as the temperature in the reactor decreased and the distance from the inlet to the reaction chamber increased, the changes in the morphology of the coal components decreased, with large standard deviations in the

mean maximum and minimum reflectance observed, as well as a decrease in the values of the true maximum reflectance and bireflectance.

The bireflectance $R_{bi}$ varied from 3.36% to 4.57%. The values of the true maximum reflectance $R_{rmax}$ determined for samples 10-1 and 10-2 reached the value corresponding to semi-graphite. Such a degree of transformation in the organic substance is confirmed by the value of the quotient $H/C < 0.15$ determined for these samples.

The values of the true maximum reflectance $R_{rmax}$ determined for samples 40-1 and 40-2 ($R_{max} > 3.5\%$ population) reached the level corresponding to semi-graphite. Such a degree of transformation in the organic substance is confirmed by the value of the quotient $H/C \leq 0.15$ determined for these samples.

The values of the true maximum reflectance determined for the gasification residue at a distance of 0.75 and 1.75 m from the reactor chamber inlet reached the value corresponding to semi-graphite regardless of the pressure applied during the experiment. This is confirmed by the value of the quotient $H/C \leq 0.15$ determined for these samples.

It was found that, as the distance from the reactor chamber inlet increased, the values of the maximum temperature acting on the coal during gasification decreased, regardless of the pressure applied during the experiment.

The true maximum temperature influencing the coal during gasification was higher than the temperature recorded by the thermocouples. The differences between the temperature recorded by the thermocouples and the temperature estimated on the basis of the reflectance measurements range from 100 to 350 °C.

The obtained results show that the distance at which the temperature effect on the coal is marked during the gasification process depends on the pressure used in the experiment. In the case of an experiment at a pressure of 10 bar, the estimated distance is approximately 60 m, while for a pressure of 40 bar, it is approximately 35 m.

**Author Contributions:** J.N. was responsible for the conceptualization, sample preparation, analysis and interpretation of results, draft manuscript preparation, writing and editing manuscript, and checking the bibliography; M.K.-P. was responsible for the analysis and interpretation of results, draft manuscript preparation, writing and editing the manuscript, and checking the bibliography; J.K. was responsible for the analysis and interpretation of results, draft manuscript preparation, writing and editing the manuscript, and checking the bibliography; M.W. was responsible for planning and carrying out the experiments, and manuscript editing and review; K.K. was responsible for planning and carrying out the experiments; Z.A. was responsible for the analysis and interpretation of results, draft manuscript preparation, writing and editing the manuscript, and checking the bibliography. All authors have read and agreed to the published version of the manuscript.

**Funding:** Coal gasification experiments presented in this paper were performed as a part of the following project: Technology Options for Coupled Underground Coal Gasification and $CO_2$ Capture and Storage, funded by the European Union's Seventh Framework Programme for Research, Technology Development and Demonstration under grant agreement no. 608517. Studies of the optical properties of coals after ex situ experiments were not funded.

**Data Availability Statement:** Not applicable.

**Conflicts of Interest:** The authors declare no conflict of interest.

## References

1. Gregg, D.W.; Edgar, T.F. Underground coal gasification. *AIChE J.* **1978**, *24*, 753–781. [CrossRef]
2. Maev, S.; Bliderman, M.S.; Gruber, G.P. Underground coal gasification (UCG) to products: Designs, efficiencies, and economics. *Undergr. Coal Gasif. Combust.* **2018**, 435–468. [CrossRef]
3. Burton, E.; Friedmann, J.; Upadhye, R. *Best Practices in Underground Coal Gasification*; Lawrence Livermore National Laboratory: Livermore, CA, USA, 2019.
4. Shafirovich, E.; Varma, A. Underground coal gasification: A brief review of current status. *Ind. Eng. Chem. Res.* **2009**, *48*, 7865–7875. [CrossRef]
5. Klimenko, A. Early Ideas in Underground Coal Gasification and Their Evolution. *Energies* **2009**, *2*, 456–476. [CrossRef]
6. Nieć, M.; Sermet, E.; Chećko, J.; Górecki, J. Evaluation of coal resources for underground gasification in Poland. Selection of possible UCG sites. *Fuel* **2017**, *208*, 193–202. [CrossRef]

7. Frejowski, A.; Bondaruk, J.; Duda, A. Challenges and Opportunities for End-of-Life Coal Mine Sites: Black-to-Green Energy Approach. *Energies* **2021**, *14*, 1385. [CrossRef]
8. Perkins, G. Underground coal gasification—Part II: Fundamental phenomena and modelling. *Prog. Energy Combust.* **2018**, *67*, 234–274. [CrossRef]
9. Kapusta, K.; Stańczyk, K.; Wiatowski, M.; Chećko, J. Environmental aspects of a field-scale underground coal gasification trial in a shallow coal seam at the Experimental Mine Barbara in Poland. *Fuel* **2013**, *113*, 196–208. [CrossRef]
10. Kasztelewicz, Z.; Ptak, K.; Zajączkowski, M. Szanse i zagrożenia podziemnego zgazowania węgla. *Przegl. Górn.* **2009**, *1–2*, 8–11.
11. Nieć, M. Barriers and limitations for underground coal gasification. *Bull. Państw. Inst. Geol.* **2012**, *448*, 183–194.
12. Nieć, M.; Chećko, J.; Górecki, J.; Sermet, E. State of the resources base of coal in Poland and deposits and environmental problems in relation to the underground coal gasification process. *Przegl. Górn.* **2014**, *11*, 28–37.
13. Palarski, J.; Strozik, G.; Jendruś, R. The influence on the rock mass deformation on the protection of the surface and ground water resources by underground coal gasification. *Przegl. Górn.* **2013**, *8*, 149–155.
14. Salamon, K.; Kabiesz, J. Selected aspects of hazards associated with the attempts of underground coal gasification. *Przegl. Górn.* **2013**, *12*, 23–31.
15. Pankiewicz-Sperka, M.; Kapusta, K.; Basa, W.; Stolecka, K. Characteristics of Water Contaminants from Underground Coal Gasification (UCG) Process—Effect of Coal Properties and Gasification Pressure. *Energies* **2021**, *14*, 6533. [CrossRef]
16. Wiatowski, M.; Kapusta, K.; Nowak, J.; Szyja, M.; Basa, W. An exsitu underground coal gasification experiment with a siderite interlayer: Course of the process, production gas, temperatures and energy efficiency. *Int. J. Coal Sci. Technol.* **2021**, *8*, 1447–1460. [CrossRef]
17. Wiatowski, M.; Stańczyk, K.; Świądrowski, J.; Kapusta, K.; Cybulski, K.; Krause, E.; Grabowski, J.; Rogut, J.; Howaniec, N.; Smoliński, A. Semi-technical underground coal gasification (UCG) using the shaft method in Experimental Mine "Barbara". *Fuel* **2012**, *99*, 170–179. [CrossRef]
18. Bhutto, A.W.; Bazmi, A.A.; Zahedi, G. Underground coal gasification: From fundamentals to applications. *Prog. Energy Combust.* **2013**, *39*, 189–214. [CrossRef]
19. Green, M. Underground coal gasification, state of the art. In Proceedings of the Clean Coal Conference'2008, Bedewo, Poland, 8 December 2008.
20. Hydrogen-Oriented Underground Coal Gasification for Europe (HUGE). European Commission Final Report 2012; EUR 25044. Available online: https://op.europa.eu/en/publication-detail/-/publication/885cb5ab-9f08-11e5-8781-01aa75ed71a1 (accessed on 15 January 2021).
21. Wiatowski, M.; Kapusta, K. Evolution of tar compounds in raw gas from a pilot-scale underground coal gasification (UCG) trial at Wieczorek mine in Poland. *Fuel* **2020**, *276*, 118070. [CrossRef]
22. Kapusta, K.; Wiatowski, M.; Stańczyk, K.; Zagoršcak, R.; Hywel Rhys, T. Large-scale Experimental Investigations to Evaluate the Feasibility of Producing Methane-Rich Gas (SNG) through Underground Coal Gasification Process. Effect of Coal Rank and Gasification Pressure. *Energies* **2020**, *13*, 1334. [CrossRef]
23. Kapusta, K. Effect of Lignite Properties on Its Suitability for the Implementation of Underground Coal Gasification (UCG) in Selected Deposits. *Energies* **2021**, *14*, 5816. [CrossRef]
24. Gabzdyl, W.; Probierz, K. The occurrence of anthracites in an area characterized by lower rank coals in the Upper Silesian Coal Basin of Poland. *Int. J. Coal Geol.* **1987**, *7*, 209–225. [CrossRef]
25. Gabzdyl, W.; Probierz, K. Thermal methamorphic products of coals from Jastrzębie Region. In Proceedings of the International Conference on Structure and Properties of Coals, Wroclaw, Poland, 17–19 June 1991; Institute of Chemistry and Technology of Petroleum and Coal, Technical University of Wroclaw: Wroclaw, Poland, 1991; pp. 7–9.
26. Probierz, K. Effect of thermal metamorphism on coalification degree (rank) and petrographic composition of the coal seams in Jastrzębie region (Upper Silesia Coal Basin of Poland). *Zesz. Nauk. Politech. Śląskiej Górnictwo* **1989**, *176*.
27. Chodyniecka, L.; Sankiewicz, J. Basalt from the Sumina area (Rybnik Coal Basin). *Geol. Q.* **1978**, *22*, 119–133.
28. Matuszewska, A.; Pusz, S.; Duber, S. Evaluation of the structure of bituminous coal from Sośnica mine in the Upper Silesian Coal Basin (Poland) using reflectance indicating surface (RIS) parameters. *Int. J. Coal Geol.* **2015**, *152*, 177–188.
29. Adamczyk, Z.; Komorek, J.; Nowak, J.; Lewandowska, M. The impact of a Neogene basaltoid intrusion on the distribution of rare earth elements and yttrium in Carboniferous rocks from the Sumina area, Poland (SW part of Upper Silesian Coal Basin). *Acta Geol. Pol.* **2020**, *70*, 31–49. [CrossRef]
30. Goodarzi, F.; Murchison, D.G. Optical properties of carbonized vitrinites. *Fuel* **1972**, *51*, 322–328.
31. Jimenez, A.; Iglesias, J.M.; Laggoun-Defarge, F.; Suarez-Ruiz, I. Effect of the increase in temperature on the evolution of the physical and chemical structure of vitrinite. *J. Anal. Appl. Pyrol.* **1999**, *50*, 117–148.
32. Murchison, D.G. Petrographic aspect of coal structure: Reactivity of macerals in laboratory and natural environments. *Fuel* **1991**, *70*, 296–315.
33. Komorek, J.; Morga, R. Charakterystyka własności optycznych witrynitu poddanego obróbce termicznej na przykładzie węgla z pokładu 833/1 kopalni Gliwice. *Zesz. Nauk. Pol. Śl. Górnictwo* **2001**, *249*, 59–73.
34. Komorek, J.; Morga, R. Vitrinite reflectance property change during heating under inert conditions. *Int. J. Coal Geol.* **2003**, *54*, 125–136. [CrossRef]

35. Komorek, J.; Morga, R.; Lewandowski, M. Własności optyczne witrynitu poddanego obróbce termicznej na przykładzie węgla z kopalni Chwałowice z GZW. *Przegl. Górn.* **2000**, *56*, 36–40.
36. Morga, R.; Komorek, J. Wpływ obróbki termicznej na własności optyczne i strukturę wewnętrzną antracytu. *Zesz. Nauk. Pol. Śl. Górnictwo* **2002**, *254*, 111–128.
37. Morga, R.; Komorek, J. *Zmienność Cech Optycznych i Struktury Witrynitu Poddanego Oddziaływaniu Temperatur w Zakresie 400–1200 °C. Monograph*; Prace Geologiczne PAN: Kraków, Poland, 2004; pp. 1–152.
38. Komorek, J.; Morga, R. Evolution of optical properties of vitrinite, sporinite and semifusinite in response to heating under inert condition. *Int. J. Coal Geol.* **2007**, *71*, 389–404. [CrossRef]
39. Komorek, J. *Zmiany Struktury Wewnętrznej Witrynitu i Liptynitu Poddanych Oddziaływaniu Temperatury w Zakresie 400–1200 °C. Monograph*; Wydawnictwo Politechniki Śląskiej: Gliwice, Poland, 2013.
40. Róg, L. Vitrinite reflectance as a measure of the range of influence of the temperature of a georeactor on rock mass during underground coal gasification. *Fuel* **2018**, *224*, 94–100. [CrossRef]
41. Malumbazo, N.; Wagner, N.J.; Bunt, J.R. The petrographic determination of reactivity differences of two South African inertinite-rich lump coals. *J. Anal. Appl. Pyrol.* **2012**, *93*, 139–146. [CrossRef]
42. Perkins, G. Underground coal gasification—Part I: Field demonstrations and process performance. *Prog. Energy Combust. Sci.* **2018**, *67*, 58–187. [CrossRef]
43. Wiatowski, M.; Kapusta, K.; Świądrowski, J.; Cybulski, K.; Ludwik-Pardała, M.; Grabowski, J.; Stańczyk, K. Technological aspects of underground coal gasification in the Experimental "Barbara" Mine. *Fuel* **2015**, *159*, 454–462. [CrossRef]
44. Khan, M.M.; Mmbaga, J.P.; Shirazi, A.S.; Trivedi, J.; Li, Q.; Gupta, R. Modelling underground coal gasification-A review. *Energies* **2015**, *8*, 12603–12668. [CrossRef]
45. *PN-ISO 7404-2:2005*; Metody Analizy Petrograficznej Węgla Kamiennego (Bitumicznego) i Antracytu—Część 2: Metoda Przygotowania Próbek Węgla. Available online: https://sklep.pkn.pl/pn-iso-7404-2-2005p.html (accessed on 15 January 2021).
46. *PN-ISO 7404-5:2002*; Metody Analizy Petrograficznej Węgla Kamiennego (Bitumicznego) i Antracytu—Część 5: Metoda Mikroskopowa Oznaczania Refleksyjności Witrynitu. Available online: https://sklep.pkn.pl/pn-iso-7404-5-2002p.html (accessed on 15 January 2021).
47. Kilby, W.E. *Biaxial Reflecting Coals in the Peace River Coalfield*; British Columbia Ministry of Energy, Mines and Petroleum, Geological Fieldwork, Paper 1986-1; British Columbia Geological Survey: Victoria, BC, Canada, 1986; pp. 127–137.
48. Kilby, W.E. Recognition of vitrinite with non-uniaxial negative reflectance characteristics. *Int. J. Coal Geol.* **1988**, *9*, 267–285. [CrossRef]
49. Kilby, W.E. Vitrinite reflectance measurement—Some technique enhancements and relationships. *Int. J. Coal Geol.* **1991**, *9*, 201–218. [CrossRef]
50. *PN-G-04560:1998*; Paliwa Stałe—Oznaczanie Zawartości Wilgoci, Części Lotnych Oraz Popiołu Analizatorem Automatycznym. Available online: https://sklep.pkn.pl/pn-g-04560-1998p.html (accessed on 15 January 2021).
51. *PN-G-04516:1998*; Paliwa Stałe—Oznaczanie Zawartości Części Lotnych Metodą Wagową. Available online: https://sklep.pkn.pl/pn-g-04516-1998p.html (accessed on 23 January 2021).
52. *PN-ISO 1928:2020-05*; Paliwa Stałe—Oznaczanie Ciepła Spalania Metodą Spalania w Bombie Kalorymetrycznej i Obliczanie Wartości Opałowej. Available online: https://sklep.pkn.pl/pn-iso-1928-2020-05e.html (accessed on 15 January 2021).
53. *PN-G-04584:2001*; Paliwa Stałe—Oznaczanie Zawartości Siarki Całkowitej i Popiołowej Automatycznymi Analizatorami. Available online: https://sklep.pkn.pl/pn-g-04584-2001p.html (accessed on 23 January 2021).
54. *PN-ISO 11760:2007*; Klasyfikacja Węgla. Available online: https://sklep.pkn.pl/pn-iso-11760-2007p.html (accessed on 15 January 2021).
55. Taylor, G.H.; Teichmüller, M.; Davis, A.; Diessel, C.K.F.; Littke, R.; Robert, T. *Organic Petrology*; Gebr. Borntraeger: Berlin, Germany; Stuttgart, Germany, 1998.
56. Malumbazo, N.; Wagner, N.J.; Bunt, J.R. The impact of particle size and maceral segregation on char formation in a packed bed combustion unit. *Fuel* **2013**, *111*, 350–356. [CrossRef]
57. Malumbazo, N.; Wagner, N.J.; Bunt, J.R.; Van Niekerk, D.; Assumption, H. Structural analysis of chars generated from South African inertinite coals in a pipe-reactor combustion unit. *Fuel Process. Technol.* **2011**, *92*, 743–749. [CrossRef]